ADVANCES IN ATMOSPHERIC SCIENCES, VOL. 31, JULY 2014, 801–813

The Natural Oscillation of Two Types of ENSO Events Based on Analyses of CMIP5 Model Control Runs

XU Kang[1,2,3], SU Jingzhi*[2], and ZHU Congwen[2]

[1]*State Key Laboratory of Tropical Oceanography, South China Sea Institute of Oceanology, Chinese Academy of Sciences, Guangzhou* 510301

[2]*Institute of Climate Systems, Chinese Academy of Meteorological Sciences, Beijing* 100081

[3]*Key Laboratory of Meteorological Disaster of Ministry of Education, Nanjing University of Information Science and Technology, Nanjing* 210044

(Received 22 July 2013; revised 16 October 2013; accepted 20 November 2013)

ABSTRACT

The eastern- and central-Pacific El Niño-Southern Oscillation (EP- and CP-ENSO) have been found to be dominant in the tropical Pacific Ocean, and are characterized by interannual and decadal oscillation, respectively. In the present study, we defined the EP- and CP-ENSO modes by singular value decomposition (SVD) between SST and sea level pressure (SLP) anomalous fields. We evaluated the natural features of these two types of ENSO modes as simulated by the pre-industrial control runs of 20 models involved in phase five of the Coupled Model Intercomparison Project (CMIP5). The results suggested that all the models show good skill in simulating the SST and SLP anomaly dipolar structures for the EP-ENSO mode, but only 12 exhibit good performance in simulating the tripolar CP-ENSO modes. Wavelet analysis suggested that the ensemble principal components in these 12 models exhibit an interannual and multi-decadal oscillation related to the EP- and CP-ENSO, respectively. Since there are no changes in external forcing in the pre-industrial control runs, such a result implies that the decadal oscillation of CP-ENSO is possibly a result of natural climate variability rather than external forcing.

Key words: EP- and CP-ENSO, CMIP5, interannual/decadal oscillation, natural variability

Citation: Xu, K., J. Z. Su, and C. W. Zhu, 2014: The natural oscillation of two types of ENSO events based on analyses of CMIP5 model control runs. *Adv. Atmos. Sci.*, **31**(4), 801–813, doi: 10.1007/s00376-013-3153-5.

1. Introduction

The El Niño-Southern Oscillation (ENSO) is the most significant interannual signal in tropical air-sea interactions, but its impacts extend far beyond the tropical region. It has been observed that there are two types of ENSO events prevailing in the tropical Pacific: one is the conventional eastern Pacific (EP) mode and the other is the central Pacific (CP) mode (Fu et al., 1986; Trenberth and Stepaniak, 2001; Larkin and Harrison, 2005; Ashok et al., 2007; Yu and Kao, 2007; Kao and Yu, 2009; Kug et al., 2009; Ren and Jin, 2011; Xu et al., 2012; Wang et al., 2012; Wang and Wang, 2013a, 2013b). The mechanism of EP-El Niño events can be mostly explained by classic ENSO theories (Bjerknes, 1969; Wyrtki, 1975; Philander et al., 1984; Schopf and Suarez, 1988; Jin, 1997a, 1997b). However, CP-El Niño events show large irregularity during their evolution, and so far at least four different mechanisms have been proposed to explain the dynamics of CP-El Niño (Ashok et al., 2009; Kug et al., 2009; Yu et al., 2010; Xiang et al., 2013).

According to observations, CP-ENSO events have become more frequent and much stronger in recent decades (Ashok et al., 2007; Ashok et al., 2009; Kao and Yu, 2009; Kug et al., 2009; Lee and McPhaden, 2010; McPhaden et al., 2011; Xu et al., 2012). Therefore, it seems logical to attribute the higher frequency of CP-El Niño events to the recent trend of global warming. On the other hand, some studies have suggested that CP-El Niño events can also be found in long-term climate records (Yeh et al., 2009; Yu and Kim, 2013; Wang and Wang, 2013a), and a decadal signal seems to be dominant in the interannual variability of CP-El Niño (Ashok et al., 2007; Weng et al., 2007; Kug et al., 2009; Choi et al., 2012; Xu et al., 2012, 2013; Xiang et al., 2013). Meanwhile, results from a number of numerical experiments have implied that CP-El Niño may be a part of natural variability in the atmosphere-ocean coupled climate system (e.g., Yu and Kim, 2010; Ham and Kug, 2011; Kim and Yu, 2012; Kug et al., 2012).

The CP-ENSO has shown a different impact on remote climate, which has provided us with a potential predictor in decadal climate forecasting. However, whether or not the fre-

* Corresponding author: SU Jingzhi
Email: sujz@cams.cma.gov.cn

quent occurrence of CP-El Niño events is a result of global warming or just natural variability in the climate system should be clearly addressed. Recently, much attention has been paid to the Coupled Model Intercomparison Project (CMIP) for the IPCC's Fifth Assessment Report. CMIP5 includes generally higher resolution models, and the model outputs tend to be super in many aspects (Taylor et al., 2012). Compared to the models included in CMIP3, the pre-industrial simulations of the CMIP5 models are better at simulating the observed characteristics of the two types of ENSO (Kim and Yu, 2012; Kug et al., 2012). However, the multi-decadal variability of CP-ENSO and its causes have yet to be properly explored in CMIP5 results

We investigated the periodicities and coupled modes of EP/CP-ENSO based on the pre-industrial control runs of CMIP5 models From the results, in the present paper we discuss the natural variability of the two types of ENSO events. Since there is no external forcing in the pre-industrial control runs, any decadal changes of ENSO can therefore be considered as natural climate variability. In this way, we aim to answer whether or not the decadal variations of EP/CP-ENSO are the result of internal interaction or external forcing in the climate system.

The remainder of the paper is organized as follows. The datasets and methods used are described in section 2. Section 3 focuses on the interannual and decadal variations of SST in the tropical Pacific. Two types of ENSO modes in the CMIP5 control runs are presented in section 4. And finally, a discussion and summary of the key findings is given in section 5.

2. Data and methodology

We focused on the pre-industrial control runs of 20 CMIP5 climate models. In these model control runs, the greenhouse gases are fixed at pre-industrial levels during the whole integration. Table 1 provides information regarding each of the models' developers and their integration periods, and the last column indicates the time period of the control runs. It can be seen that the time period of each model control run is different, and some models, such as BCC-csm1-1, CNRM-CM5, FGOALS-g2, FGOALS-s2, HadGEM2-ES, inmcm4, and MIROC5, also demonstrate apparent discontinuity and instability during their full record lengths (data not shown). Therefore, to find a stable benchmark time period in the control runs, we firstly calculated the global area-weighted mean SST, and defined one standard deviation (STD) of its time series as a criterion to evaluate model stability. The STD was calculated for a moving 200-yr period in each model control run, and the "most stable" 200-yr period was defined as the benchmark and used in our analysis (see the last column of Table 1). It was noted that the model CESM1-WACCM only has a 200yr run; and as a result for this model we retained the whole time period for analysis.

The observed monthly SST data used in the study were derived from the Met Office Hadley Centre Sea Ice and Sea Surface Temperature (HadISST) dataset, which is gridded at $1.0^\circ \times 1.0^\circ$ for the period 1870–2010 (Rayner et al., 2003); and the sea level pressure (SLP) data for the same period were from the Met Office Hadley Centre (HadSLP2) dataset. This dataset is a unique combination of monthly globally-complete fields of land and marine pressure observations on a $5.0^\circ \times 5.0^\circ$ grid (Allan and Ansell, 2006).

In the present study, model anomalies were defined as deviations from the model climatology, which was defined by the average of 200 years in the model control runs. The anomaly correlation coefficient (ACC) was used to indicate the pattern correlation between model-simulated (s) and observed (o) values, which is defined as

$$\mathrm{ACC} = \frac{\sum_{i=1}^{N} w_i (s_i - \overline{s})(o_i - \overline{o})}{\sqrt{\sum_{i=1}^{N} w_i (s_i - \overline{s})^2 \sum_{i=1}^{N} w_i (o_i - \overline{o})^2}},$$

where an over bar indicates time average, w is area weight, and subscript i is grid point. The ACC indicated a skill score of spatial similarity between CMIP5 model simulations and the observation map. The ACC ranges from -1.0 to 1.0; and if a model simulation was close to the observation, then the ACC score would be closer to 1.0. Besides ACCs, the signal-to-error ratio (SER) was also utilized to evaluate model performance, which is defined by

$$\mathrm{SER} = \frac{1}{N} \sum_{i=1}^{N} \frac{w_i |o_i - s_i|}{w_i o_i},$$

where o is the STD of the observed SST, s is the STD of the model-simulated SST, w is area weight, and subscript i is grid point. The SER indicated the total amount of spatial difference between the model simulations and the observation map. i.e., a low SER value would demonstrate greater similarity between the simulated and observed SST anomalies fields. In addition, wavelet analysis, the Butterworth filter, and singular value decomposition (SVD) were applied as part of our statistical analyses.

3. Variations of SST anomalies in the tropical Pacific

To evaluate how well the SST variability in the tropical Pacific is simulated in the model control runs, we firstly calculated the STD fields of the observed and simulated annual SST anomalies (SSTAs) over the tropical Pacific (Fig. 1). It was found that the variances of the observed ENSO-related SSTAs primarily occur in the equatorial Pacific (10°S–10°N), extending from the coast of South America into the central equatorial Pacific. There exists another large STD center in the subtropical North Pacific, southwest to the coast of North America. Such observed variances of SSTAs seem to be well captured by most of the models, but the amplitudes of STD between the models and the observation still show some significant differences, especially in the equatorial Pacific region (Fig. 1).

Table 1. Model descriptions in CMIP5 archives. (See complete "Modeling Groups and their Terms of Use": http://cmip-pcmdi.llnl.gov/cmip5/terms.html.)

Model number	CMIP ID (label in figures)	Modeling group	AGCM resolution (Lon × Lat, vertical)	OGCM resolution (Lon × Lat, vertical)	Integration period (selected period) units: yr
1	BCC-csm1-1	Beijing Climate Center, China Meteorological Administration, China	2.81° × 2.75°, L26	1.00° × (0.33°–1.00°), L40	500 (207–406)
2	CCSM4	National Center for Atmospheric Research, USA	1.25° × 0.90°, L26	1.11° × (0.27°–0.54°), L60	500 (268–467)
3	CESM1-BGC	Community Earth System Model Contributors, USA	1.25° × 0.90°, L26	1.11° × (0.27°–0.54°), L60	500 (287–486)
4	CESM1-FASTCHEM	Community Earth System Model Contributors, USA	1.25° × 0.90°, L26	1.11° × (0.27°–0.54°), L60	222 (16–215)
5	CESM1-WACCM	Community Earth System Model Contributors, USA	1.25° × 0.90°, L26	1.11° × (0.27°–0.54°), L60	200 (1–200)
6	CNRM-CM5	Centre National de Recherches Météorologiques/Centre Européen de Recherche et Formation Avancée en Calcul Scientifique France	1.41° × 1.40°, L31	1.00° × 0.33° at equator L42	850 (292–491)
7	FGOALS-g2	LASG, Institute of Atmospheric Physics, Chinese Academy of Sciences and CESS, Tsinghua University, China	2.81° × 2.79°, L26	1.00° × (0.50°–1.00°), L30	900 (696–895)
8	FGOALS-s2	LASG, Institute of Atmospheric Physics, Chinese Academy of Sciences, China	2.81° × 1.66°, L26	1.00° × (0.50°–1.00°), L30	500 (93–292)
9	GFDL-ESM2G	NOAA Geophysical Fluid Dynamics Laboratory, USA	2.50° × 2.00°, L24	1.00° × 0.86°, L63	500 (104–303)
10	GFDL-ESM2M	NOAA Geophysical Fluid Dynamics Laboratory, USA	2.50° × 2.00°, L24	1.00° × 0.90°, L50	500 (139–338)
11	GISS-E2-H	NASA Goddard Institute for Space Studies, USA	2.50° × 2.00°, L40	2.50° × 2.00°, L33	480 (249–448)
12	HadGEM2-CC	Met Office Hadley Centre, United Kingdom	1.875° × 1.25°, L60	1.00° × (0.30°–1.00°), L40	240 (6–205)
13	HadGEM2-ES	Met Office Hadley Centre, United Kingdom	1.875° × 1.25°, L38	1.00° × (0.30°–1.00°), L40	575 (16–215)
14	inmcm4	Institute for Numerical Mathematics, Russia	2.00° × 1.50°, L21	1.00° × 0.50°, L40	500 (300–499)
15	IPSL-CM5A-LR	Institut Pierre-Simon Laplace, France	3.75° × 1.89°, L39	2.00° × 2.00°, L31	1000 (457–656)
16	IPSL-CM5A-MR	Institut Pierre-Simon Laplace, France	2.50° × 1.27°, L39	2.00° × 2.00°, L31	300 (81–280)
17	MIROC5	Atmosphere and Ocean Research Institute (The University of Tokyo), National Institute for Environmental Studies, and Japan Agency for Marine-Earth Science and Technology, Japan	1.40° × 1.40°, L40	1.40° × (0.50°–1.40°), L50	670 (159–358)
18	MPI-ESM-LR	Max Planck Institute for Meteorology Germany	1.875° × 1.875°, L47	1.50° × 0.82°, L50	1000 (744–943)
19	MRI-CGCM3	Meteorological Research Institute, Japan	1.125° × 1.125°, L48	1.00° × 0.50°, L51	500 (91–290)
20	NorESM1-M	Norwegian Climate Centre, Norway	2.50° × 1.895°, L26	0.94° × (0.50°–1.00°), L53	500 (35–234)

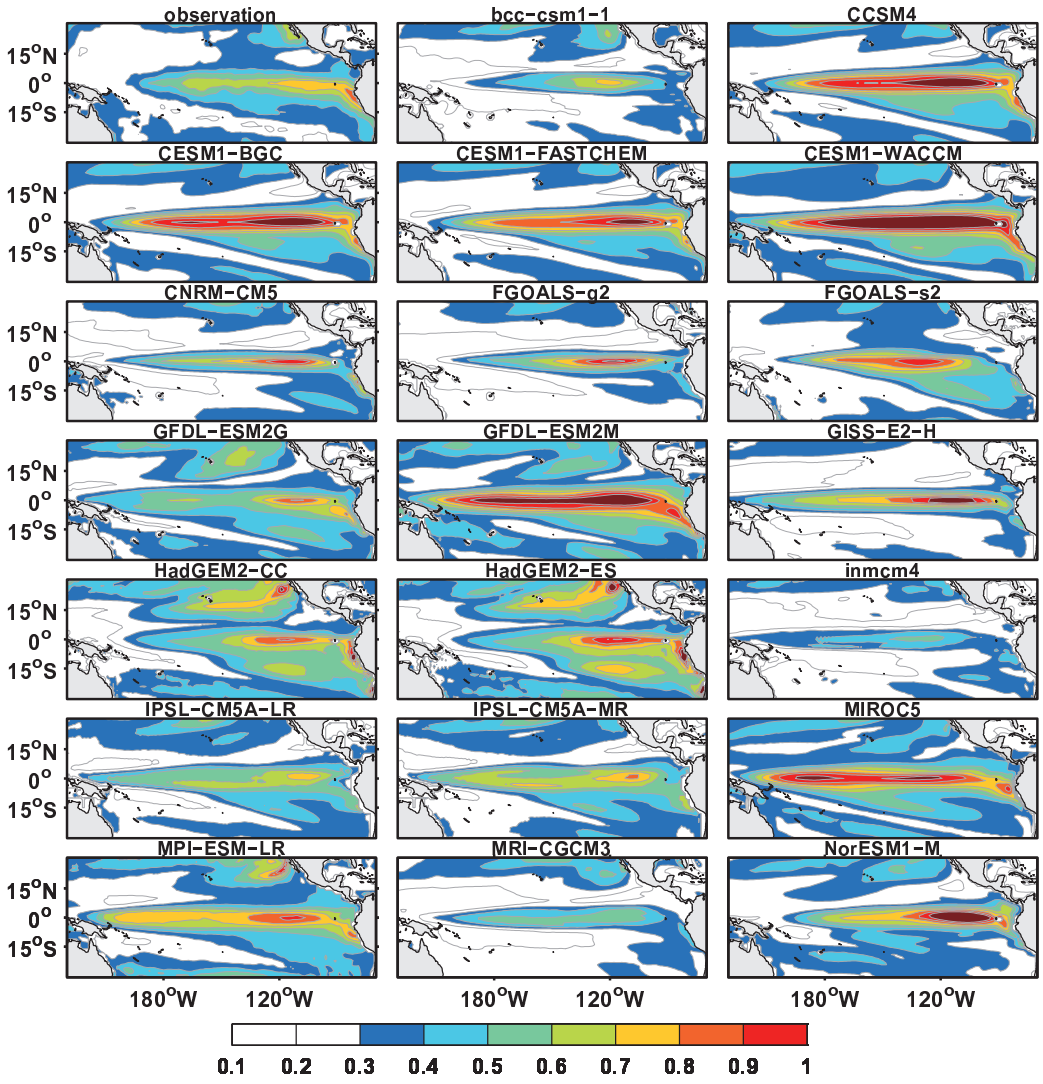

Fig. 1. Spatial patterns of standard deviation (STD) of annual sea surface temperature (SST) for the observation and 20 models in CMIP5. Color shaded regions represent the STD exceeding 0.3°C.

The ACCs between model-simulated and observed annual SSTAs in the STD fields varied from 0.57 (inmcm4) to 0.83 (CCSM4) over the tropical Pacific region (30°S–30°N), and the ensemble mean of ACCs was 0.72. Fifteen of the models can realistically simulate the major maximum centers of observed SSTA variances. We noted that the ACCs related with all these 15 models were greater than 0.66, and hence a criterion of 0.66 can be used to evaluate the abilities of model simulations. It is worth noting that the ACC between GISS-E2-H and the observation was 0.74, but it fails to simulate the observed SST variances in the subtropical North Pacific. In addition, the BCC-csm1-1 (with an ACC of 0.62) and MIROC5 (with an ACC of 0.65) model-simulated SSTA variability centers in the equatorial Pacific are more westward than observed, and the inmcm4 (with an ACC of 0.57) and MRI-CGM3 (with ACC of 0.62) model-simulated SSTA variances are much weaker than observed.

A number of studies have suggested that EP-El Niño events mainly exhibit an interannual variability while CP-El Niño events are characterized by decadal variation (Ashok et al., 2007; Weng et al., 2007; Kug et al., 2009; Choi et al., 2012; Xu et al., 2012; Xiang et al., 2013). To evaluate the performance of the models in simulating SSTAs on the interannual and decadal time scales, we applied a high-pass filter to the SSTA fields and obtained the interannual (< 8 years) components. Meanwhile, we also applied a low-pass filter to the SSTA fields, and obtained the decadal (> 8 years) components. The STD fields of the observed and model-simulated interannual SSTs are displayed in Fig 2. The results suggest that the spatial pattern of observed SST variability in the equatorial Pacific on the interannual time scale is analogous to the unfiltered counterpart; it is characterized by a maximum center of STD in the eastern equatorial Pacific, but with a weaker intensity. Most (90%) of the models can capture the spatial pattern of the interannual variability of SSTAs, with ACC values larger than 0.7. However, two of the models (inmcm4 with an ACC of 0.61 and MRI-CGCM3 with an ACC of 0.67) failed to simulate the observed interannual SST pat-

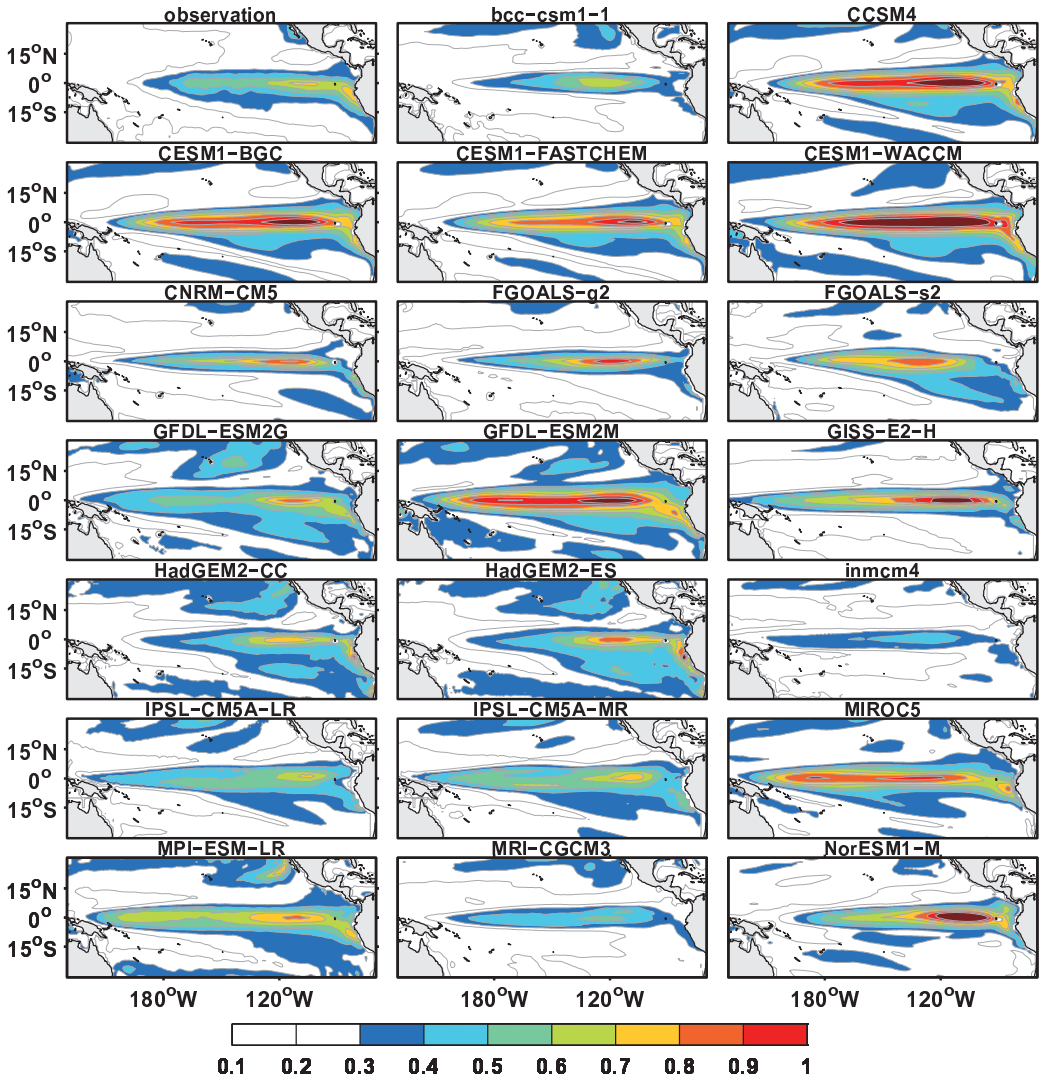

Fig. 2. The same as Fig. 1, but for the interannual (< 8 yr) component of annual SST.

terns, possibly due to the weaker variability of the simulated interannual SSTAs in the equatorial Pacific.

Figure 3 depicts the STD patterns of decadal SST for the observation and simulations. As can be seen, there are three maximum centers in the STD field for observed decadal SST: the central equatorial Pacific (between 160°E and 150°W), the eastern equatorial Pacific and the subtropics in the North Pacific southwest to the coast of North America. Compared with the interannual variability (Fig. 2), the STD of the interdecadal observed SSTAs (Fig. 3) shows a relatively larger variation in the central equatorial Pacific and the subtropical regions. Such an observed pattern indicates that the CP-El Niño is related with the subtropical variability, which is consistent with previous studies (Yu et al., 2010). More than half of the models (CCSM4, CESM1-BGC, CESM1-FASTCHEM, CESM1-WACCM, FGOALS-s2, GFDL-ESM 2M, IPSL-CM5A-LR, IPSL-CM5A-MR, MIROC5, MPI-ESM-LR and NorESM1-M) are able to capture the spatial pattern of observed SST variability on decadal time scales, especially the two maximum centers in the central equatorial Pacific and the subtropical region.

Figure 4 shows the ACCs and SERs of the STD fields between the observed and model-simulated annual SSTAs in the tropical Pacific (averaged between 30°S and 30°N) on interannual and decadal time scales. We noted that the ACCs (SERs) of the unfiltered and the interannual SSTA fields were maintained at a substantially high (low) level, while the ACCs (SERs) of decadal SSTA fields were much lower (higher) with uneven values. Therefore, the unfiltered and the filtered model-simulated SSTAs on the interannual time scale were consistent with the observation (Figs. 1 and 2), which implies that the CMIP5 models are successful in capturing the interannual variations of the annual observed SST in the tropical Pacific.

In the case of the decadal time scale, the lower ACCs (higher SERs) indicated poorer performance of the models in simulating the decadal variation of SST. However, we noted that the ACCs on the decadal time scale in nine mod-

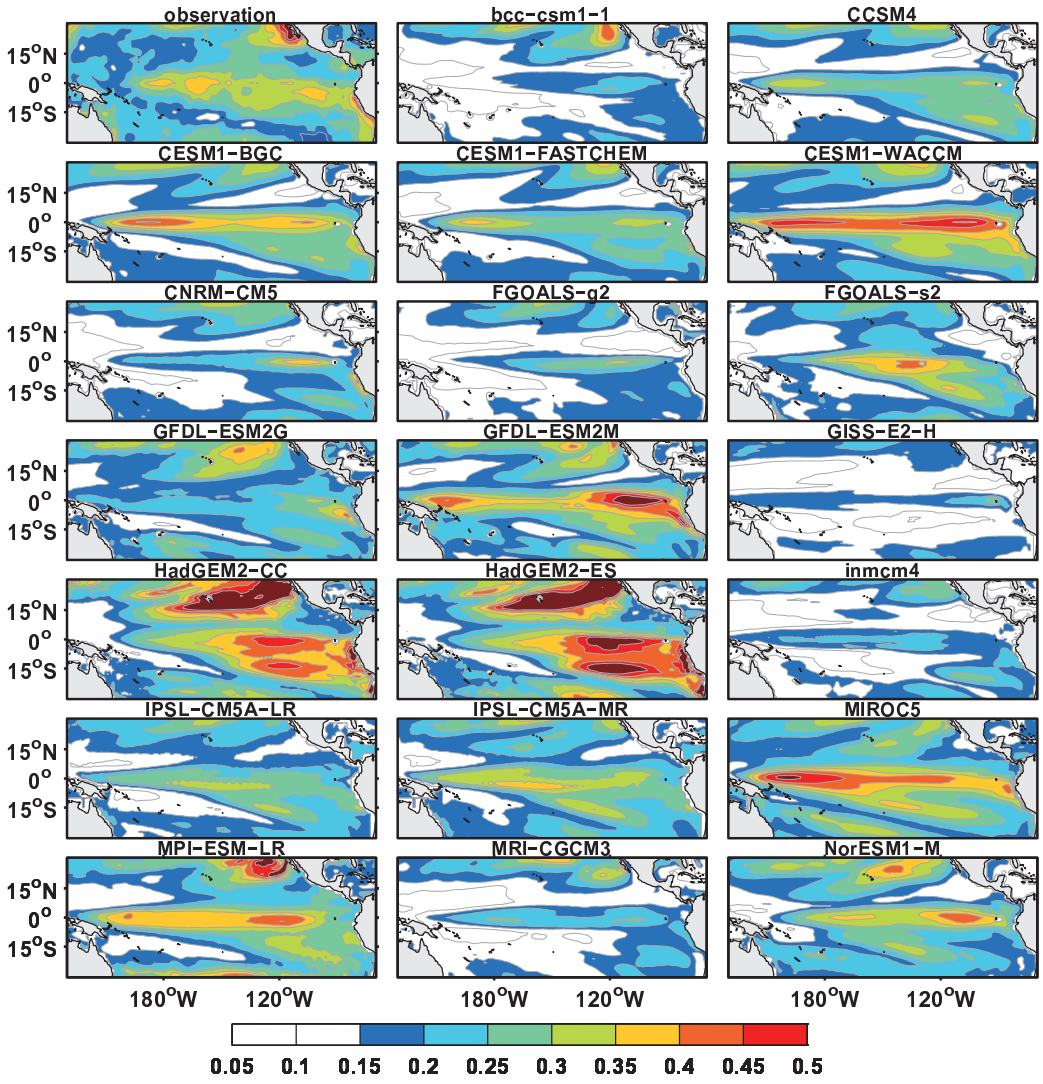

Fig. 3. The same as Fig. 1, but for the decadal (> 8 yr) component of annual SST, and color shaded regions represent the STD exceeding 0.15°C.

els (CCSM4, CESM1-BGC, CESM1-FASTCHEM, CESM1-WACCM, FGOALS-s2, GFDL-ESM2M, IPSL-CM5A-LR, IPSL-CM5A-MR and MPI-ESM-LR) were greater than 0.45 (see Fig. 4a), suggesting that the decadal variations of SSTAs can also be captured by these models. Nonetheless, the decadal ACCs in MIROC5 and NorESM1-M were 0.33 and 0.34, respectively, but these two model-simulated SSTA patterns were very close to the observation (Fig. 3). In addition, the SERs in these 11 models on the decadal time scale were all less than 0.3 (see Fig. 4b), meaning these models show good performance in simulating the SST variation on the decadal time scale in the tropical Pacific.

The time series of SST anomalies averaged in the region of Niño3 (5°S–5°N, 150°–90°W) and Niño4 (5°S–5°N, 160°E–150°W) are usually utilized to evaluate the variation of EP- and CP-ENSO events, respectively. To explore the period of SST variation in the central and eastern Pacific, we applied wavelet analysis to the time series of Niño3 and Niño4 indices in the observation and the CMIP5 models (Figs. 5 and 6) The observed Niño3 and Niño4 indices clearly exhibit a significant 2–7-yr interannual oscillation, which has been discussed previously in a number of other studies (e.g., Rasmusson and Carpenter, 1982; Battisti and Hirst, 1989; Weng et al., 2007; Kao and Yu, 2009; Wang et al., 2009; Xu et al., 2012). Such characteristics are well depicted by the CMIP5 models.

Recent studies noted that there exists a prominent decadal signal in the time series of CP-El Niño (Weng et al., 2007; Kug et al., 2009; Yeh et al., 2009; Choi et al., 2012; Xu et al., 2012, 2013). The observed Niño4 index shows a remarkable 2–7-yr oscillation, similar to those of Niño3 index. Besides this, the variability of Niño4 index also shows a remarkable 10-15-yr oscillation (see Fig. 6). We found that 14 (70%) of the 20 models (CESM1-BGC, CESM1-FASTCHEM, CESM1-WACCM, FGOALS-s2, GFDL-ESM2G, GFDL-ESM2M, HadGEM2-CC, HadGEM2-ES, IPSL-CM5A-LR, IPSL-CM5A-MR, MIROC5, MPI-ESM-LR, MRI-CGCM3 and NorESM1-M) show the capability to simulate the ob-

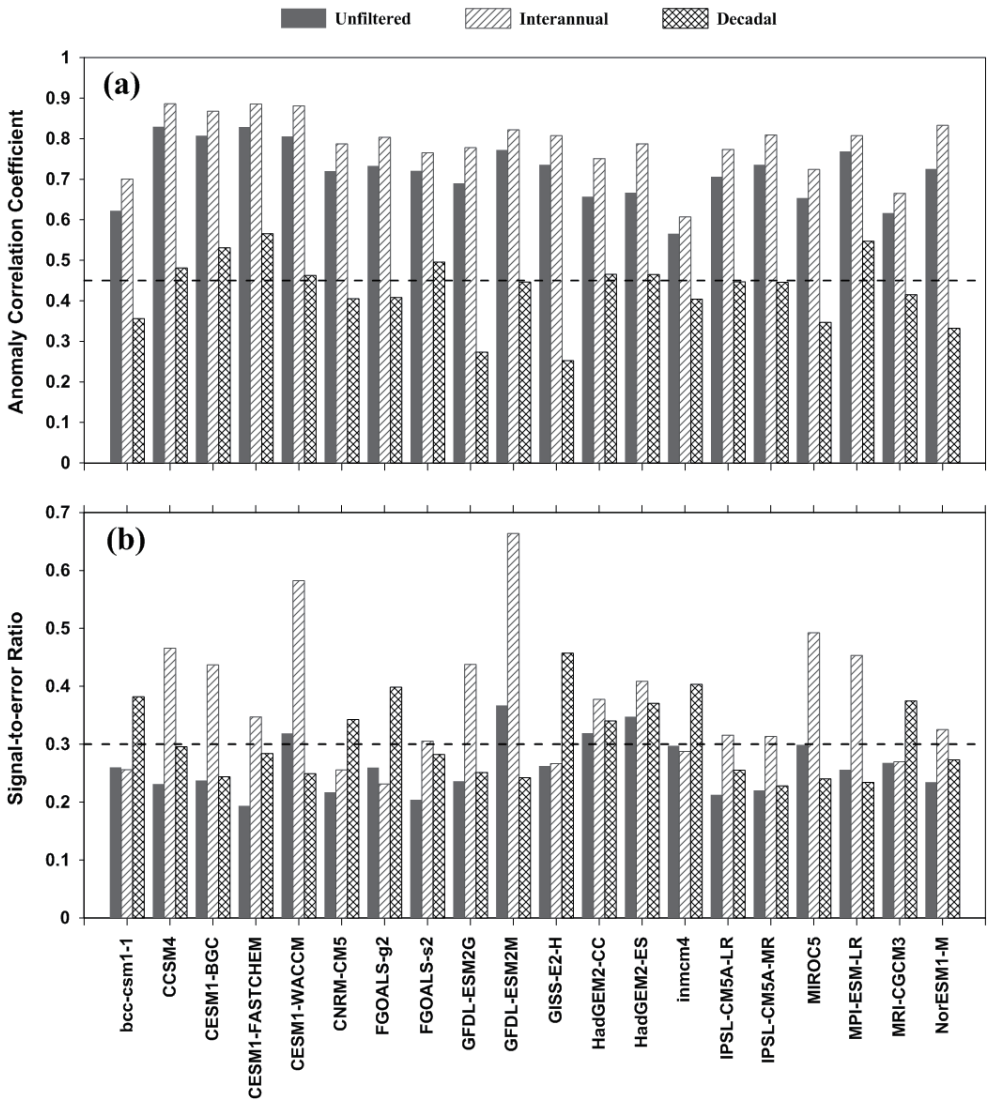

Fig. 4. (a) The anomaly correlation coefficients (ACCs) and (b) signal-to-error ratios (SERs) of the annual SSTA standard deviation in the tropical Pacific (averaged between 30°S and 30°N) between the model simulations and observation. Gray, diagonal-patterned and checked bars represent the unfitered, interannual and decadal SST, respectlively.

served interannual and decadal oscillations of Niño4 index. However, the model-simulated decadal signals of Niño4 index are not significant in BCC-csm1-1, GFDL-ESM2G, HadGEM2-CC, HadGEM2-ES and MRI-CGCM3 due to the weaker decadal STD in Niño4 region in these models (Fig. 3). In addition, the westward shift of centers of SSTAs in CCSM4 may also cause a failure to simulate the STD of decadal Niño4 SSTAs (see Fig. 3). Generally, more than half (70%) of the models in CMIP5 are able to simulate the decadal SST oscillation in the Niño4 region.

4. Two types of ENSO modes in the models

The ENSO shows a distinct atmosphere-ocean interaction, which is characterized by close coupled patterns between the tropical SST and SLP anomalous fields. Xu et al. (2013) emphasized that two types of El Niño events have different responses to the Southern Oscillation. The coupled modes of SST and SLP for EP- and CP-ENSO can clearly be seen in the SVD modes of the observed monthly SST and SLP anomalies by the first and second mode, respectively (Fig. 7). Before applying the SVD analysis, the linear trend of all fields in the observation and CMIP5 model simulations was removed.

The EP-El Niño is generally characterized by a traditional dipole of SSTAs, with warming centers in the eastern–central equatorial Pacific and a cooling center in the western tropical Pacific (the first column of Fig. 7). Similarly, the EP-Southern Oscillation (SO) is characterized by a zonal dipole of SLP anomalies in the tropics and subtropics. The positive and negative centers dominate in the Asia-Indian-Pacific junction and the eastern Pacific respectively, and they are di-

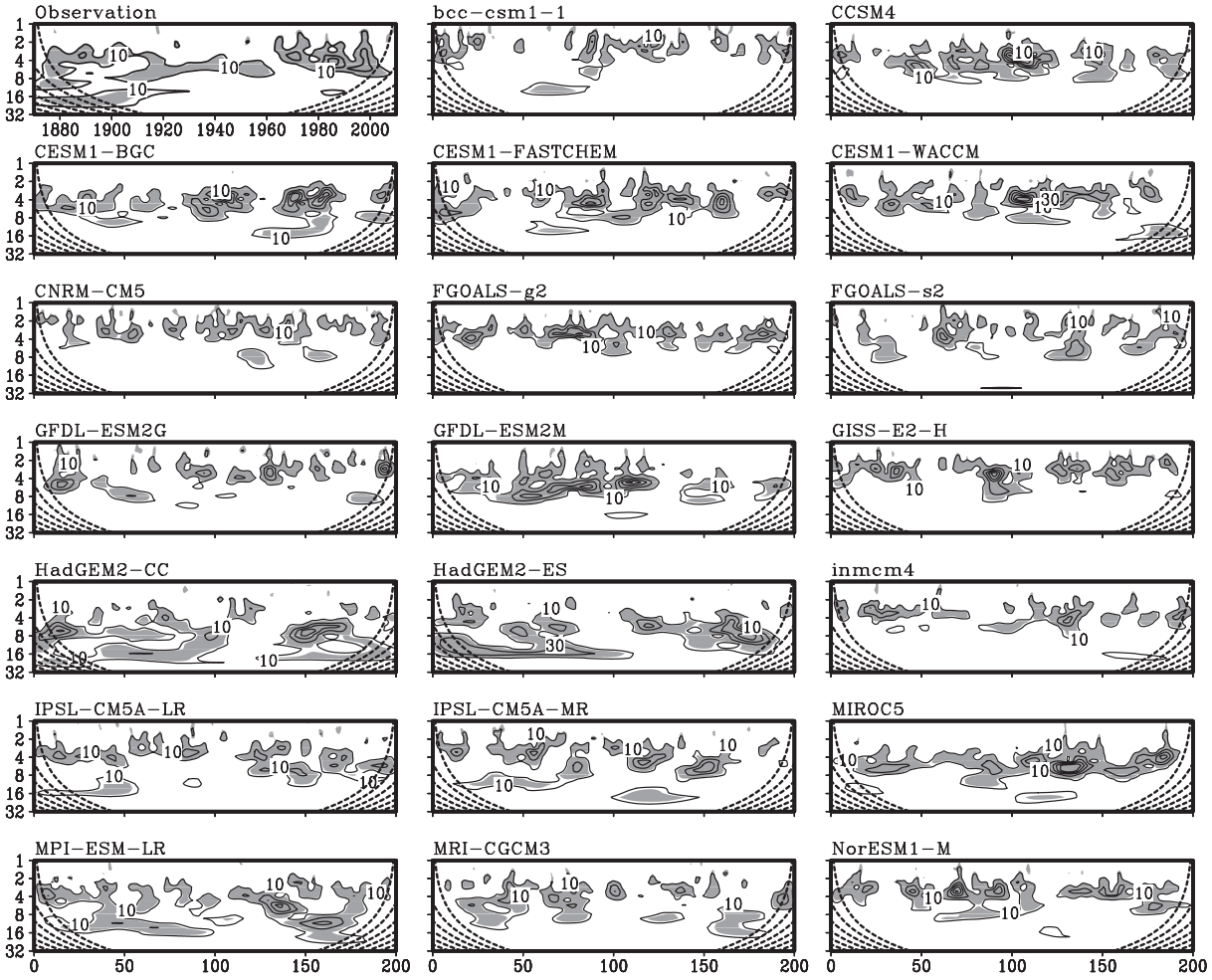

Fig. 5. The wavelet analysis of the Niño3 index, calculated on the basis of the observation and model simulations. The left axis is the Fourier Period (years) and the bottom axis is time (years). The shaded area designates statistical significance at the 95% confidence level against the red noise process, and the regions of dashed lines on either end indicate the "cone of influence", where edge effects become important.

vided by the dateline (the second column of Fig. 7). The second SVD mode suggests that the warming center in the observed CP-El Niño is mainly in the central Pacific, extending into the subtropics in both hemispheres, with cold SSTAs prevailing in the eastern and the western tropical Pacific. The observed CP-SO in the SLP anomalous field exhibits a tripolar structure, with two positive centers in the eastern tropical Indian and the eastern tropical Pacific associated with a negative center in the central tropical Pacific. Therefore, we can define the EP- and CP-ENSO modes by the SVD analyses between SST and SLP anomalous fields, and used these criteria to determine whether a particular model can simulate the ENSO modes well or not.

We noted some discrepancies (e.g., amplitude, center position) in the SVD modes between the simulations and observation. Almost all the models can reproduce the mode of EPEl Niño and the SO in the tropical Pacific. For CP-ENSO, most models can simulate CP-El Niño patterns in the second SVD mode of the SST anomalous field. However, it seems that the models can barely simulate both the observed CP-El Niño and CP-SO modes as a whole. We found that only 12 (60%) models (CCSM4, CESM1-BGC, CESM1-FASTCHEM, CESM1-WACCM, CNRM-CM5, FGOALS-g2, GFDL-ESM2G, GFDL-ESM2M, HadGEM2-CC, Had GEM2-ES, MIROC5, and NorESM1-M) can simulate both the CP-El Niño and its associated SO pattern, and five models (FGOALS-s2, GISS-E2-H, IPSL-CM5A-LR, IPSL-CM5A-MR, and MPI-ESM-LR) fail to capture the CP-El Niño and the SO pattern (the last two columns of Fig. 7). BCC-csm1-1 and MRI-CGCM3 are able to reproduce the CP-El Niño, but fail to simulate the observed CP-SO patterns. Additionally, the tripolar pattern of CP-SO seems to be well-simulated by inmcm4, but the warming center of SSTAs simulated by this model is mainly in the western Pacific warm pool, which is too far west in contrast to the observation.

Figure 8 shows the ACCs between the SVD modes in the observation and the model simulations in the case of the two ENSO modes. It shows that the mean of ACCs in the El Niño and SO fields were 0.86 and 0.91 in the case of EP-ENSO. In the CP-ENSO case, however, the means of ACCs were only 0.60 and 0.61 in the El Niño and SO fields, respectively. These results suggest that the

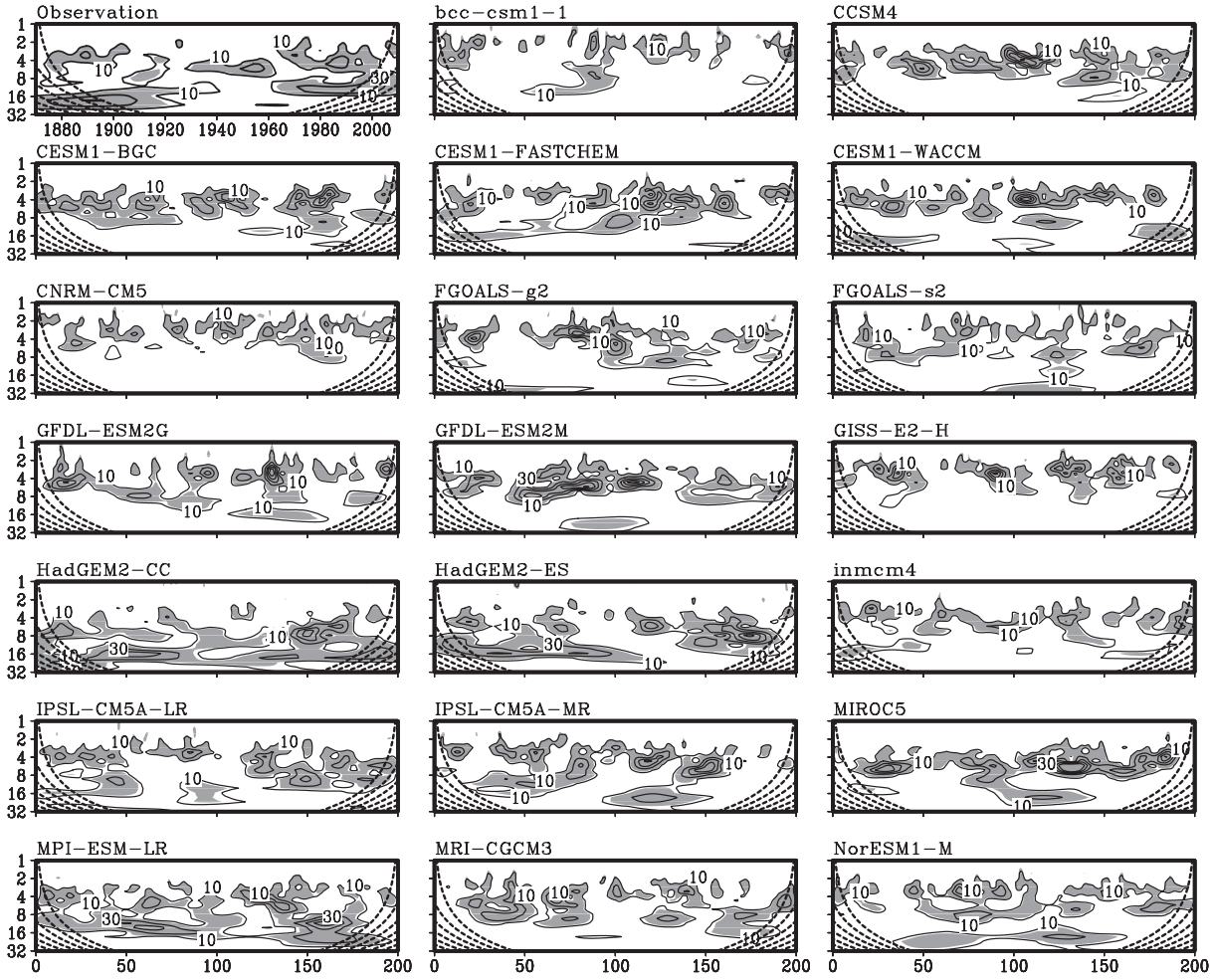

Fig. 6. The same as Fig. 5, but for the Niño4 index.

current models show relatively better performance in simulating the EP-ENSO modes than the CP-ENSO modes. When we applied the value of 0.65 as a threshold to evaluate model capability, we found that there are 12 models that can simulate both the observed EP- and CP-ENSO modes well (Fig. 7). Therefore, we chose these models (CCSM4, CESM1-BGC, CESM1-FASTCHEM, CESM1-WACCM, CNRM-CM5, FGOALS-g2, GFDL-ESM2G, GFDL-ESM2M, HadGEM2-CC, HadGEM2-ES, MIROC5 and NorESM1-M) as multi-model ensembles (MMEs) to reveal the variations of the two types ENSO events, and the results are now analyzed in the remaining part of this section.

The variations of the two types ENSO events could be evaluated by the EP and CP-El Niño indices, which are defined by the first two principal components (PC1 and PC2) in the SST field (Xu et al., 2012). It was found that these two indices exhibit a 2–7 yr and 10–15 yr oscillation corresponding to the EP- and CP-ENSO mode, respectively (Fig. 9). To validate the dominating time periods in the time variations of EP and CP-El Niño events, we calculated the MME of the global power spectrum of PC1 and PC2 (Fig. 9). In general, the model-simulated periodicity of EP and CP-El Niño shows a similar feature as we have seen in the observation. However, the global power spectrum of PC1 suggests that only an interannual oscillation is dominant in the MME, but the observed counterpart exhibits significant interannual and decadal oscillations. In the case of PC2 analysis, the results suggest that both the MME and the observation exhibit remarkable multi-decadal oscillations corresponding to the CP-Niño mode. In addition, we performed a power spectral analysis to each model-simulated CP-El Niño in CMIP5. The wavelet power spectrums suggest that all the above 14 models can reproduce the characteristics of multi-decadal oscillations, although some of the model results are not significant. This result agrees with the multi-model ensemble (data not shown), which implies that the CP-ENSO mode and oscillation can be simulated by more than half of the models in CMIP5.

The above analyses suggest that the CP-ENSO mode could potentially be simulated by some of the models during their pre-industrial control runs, and the simulated CP-ENSOs are dominated by multi-decadal oscillations, which is consistent with the observation. Since there are no signals of global warming in the pre-industrial control runs, the multi-decadal variations of simulated CP-ENSO can be regarded as natural oscillations in the climate system. Therefore, the

frequent occurrence of CP-ENSO in recent decades does not mean that CP-ESNO is the result of global warming. In fact, the CP-ENSO has been observed to be dominant before the recent trend in global warming (Giese and Ray, 2011).

5. Summary and discussion

The EP- and CP-ENSO have been found to be dominant in the tropical Pacific, at interannual and decadal time scales, respectively. In the present study, we chose 20 CMIP5 climate models to evaluate their capabilities in simulating two types of ENSO modes on the basis of pre-industrial control runs. There are no external forcing changes in these control runs; hence, the variability related to the two types of ENSO in those control runs could be treated as natural variability. It was found that most of the models (18 out of 20) in CMIP5 can realistically simulate the interannual observed SST variances in the equatorial Pacific, but only half of the models (11 out of 20) can simulate the variances of SSTAs on the decadal time scale. The variation of CP-ENSO defined by the time series of SSTAs in Niño4 shows significant decadal variation in about 70% of the models. These results support the conclusion that the interannual-decadal (decadal) variation of EP-El Niño (CP-El Niño) is a natural variability in the climate system.

Two types of ENSO events exhibit atmosphere-ocean in-

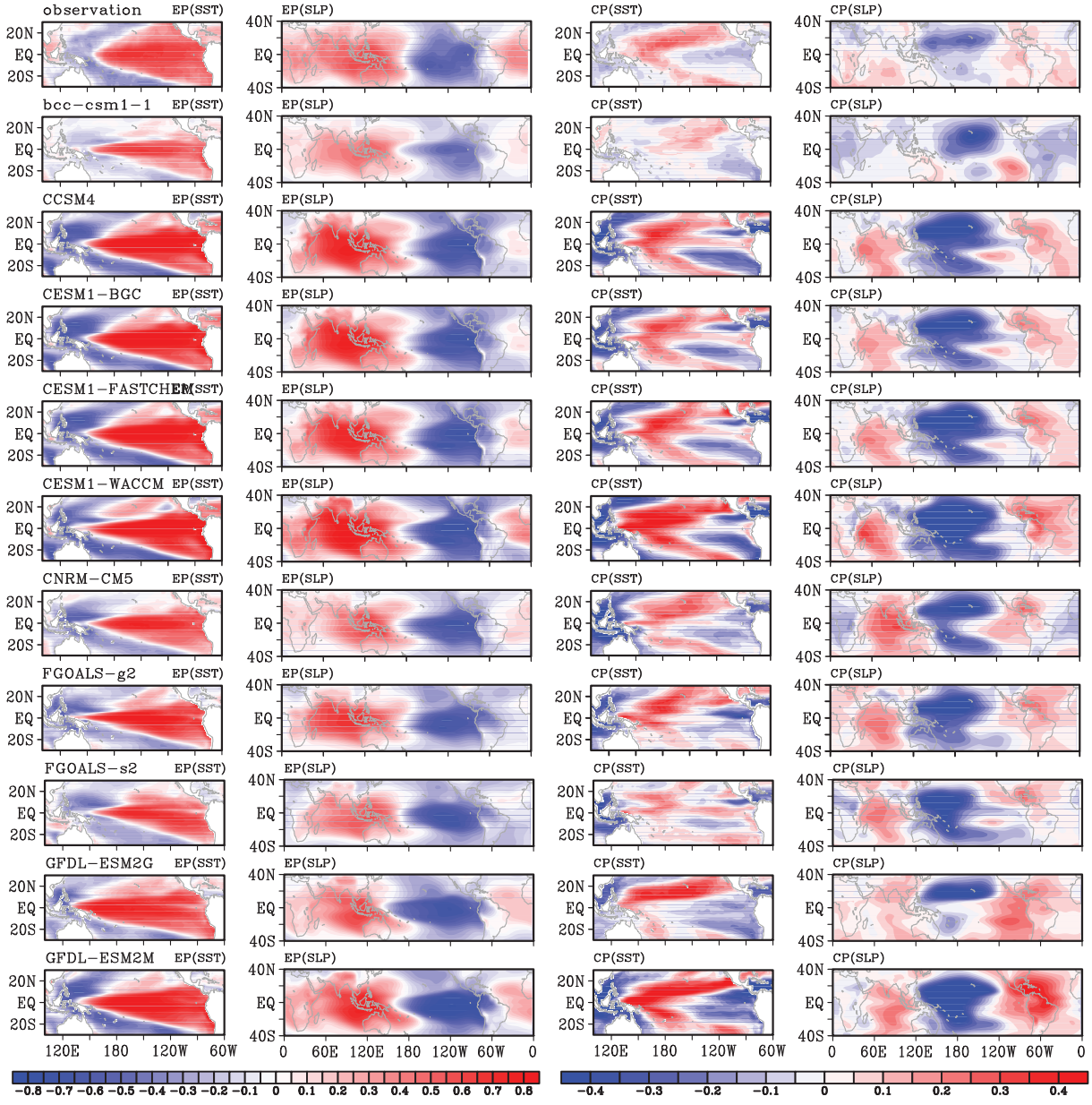

Fig. 7. Spatial patterns of the first two SVD modes of SST and SLP anomalous fields for the EP- and CP-ENSO, calculated on the basis of the observation and model control runs. The first (last) two columns show the EP-El Niño (CP-El Niño) in the SST anomalous field and EP-SO (CP-SO) in the SLP anomalous field, respectively.

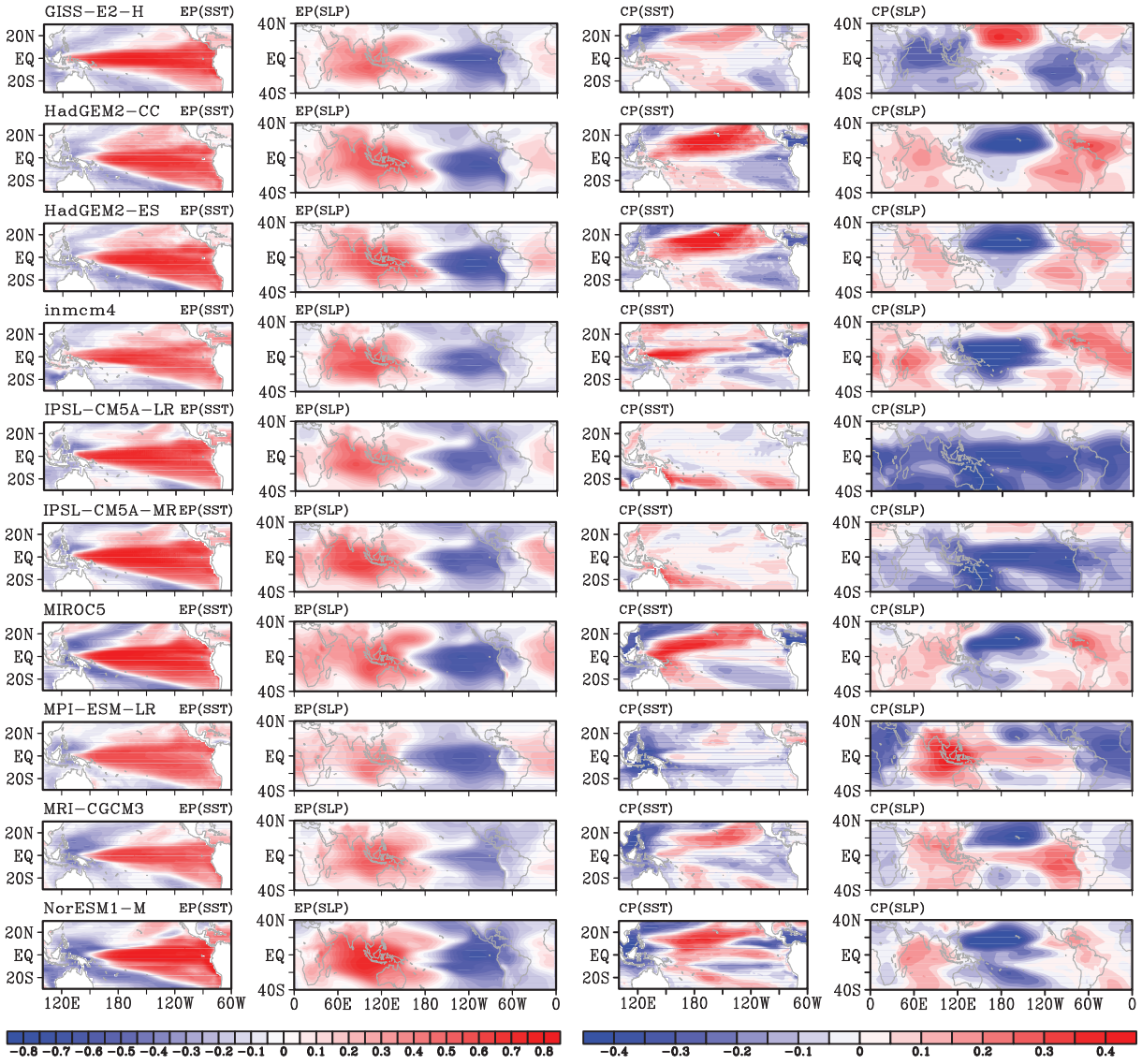

Fig. 7. (continued)

teraction on the interannual and decadal time scales, which are characterized by the coupled modes between the SST and SLP anomalies in the tropical Pacific. The SVD analyses suggested that all the model simulations in the control runs can capture the EP-ENSO modes, while the CP-ENSO modes are well simulated by only 12 models. The wavelet analysis of the first two PCs based on a 12-model ensemble indicated that the model-simulated EP-ENSO mode exhibits an interannual variability, and the decadal oscillation is found to be dominant in the variation of the CP-ENSO mode, which is consistent with observations. Therefore, both the EP- and CP-ENSO exhibit natural variability in the pre-industrial control runs, suggesting a natural variability in the climate system.

However, Kim and Yu (2012) suggested that the responses of the two types of ENSO to increases in CO_2 concentrations are different. They noted that the intensity of CP-ENSO increases gradually from the pre-industrial simulation to the historical simulation, and toward the RCP4.5 projection, while the intensity of EP-ENSO increases firstly, and then decreases from the historical simulation to the RCP4.5 projection. Therefore, changes in external forcing (e.g. GHG-forcing, aerosol-forcing) may play a role in the decadal variations of CP-El Niño in terms of its frequency and amplitude. The observed higher frequency of CP-ENSO during recent decades may be the result of joint impacts of both natural atmosphere-ocean interactions and changes in external forcing. In particular, some of the CMIP5 models fail to capture the observed CP-ENSO features in the pre-industrial control run; but how do they perform in the historical simulations and RCP projections? These issues are worth examining in future studies.

In addition, it should also be noted that there are probably differences in the atmosphere-ocean coupled physics between models, and that the coupled modes of EP/CP-ENSO also may not be the same in all of the models. This is the reason why some models (e.g., MPI-ESM-LR) can simulate the decadal variation of the tropical SST but fail to capture the atmosphere-ocean coupled modes of CP-ENSO.

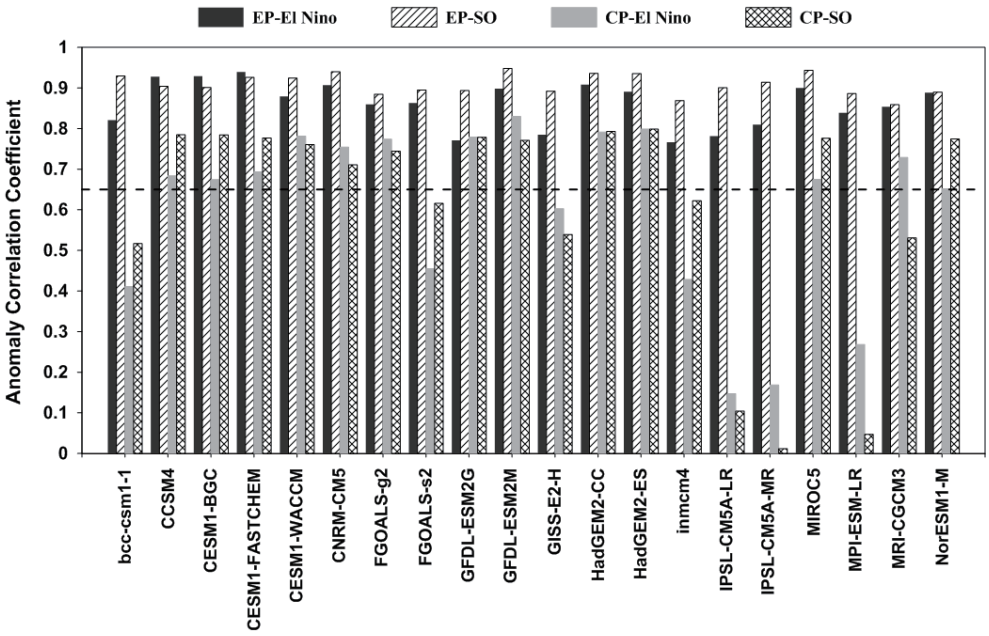

Fig. 8. The ACCs of the two types of El Niño and SO between the observation and the 20 CMIP5 models. Black (diagonal-patterned) bars represent EP-El Niño (EP-SO) and gray (checked) bars represent CP-El Niño (CP-SO).

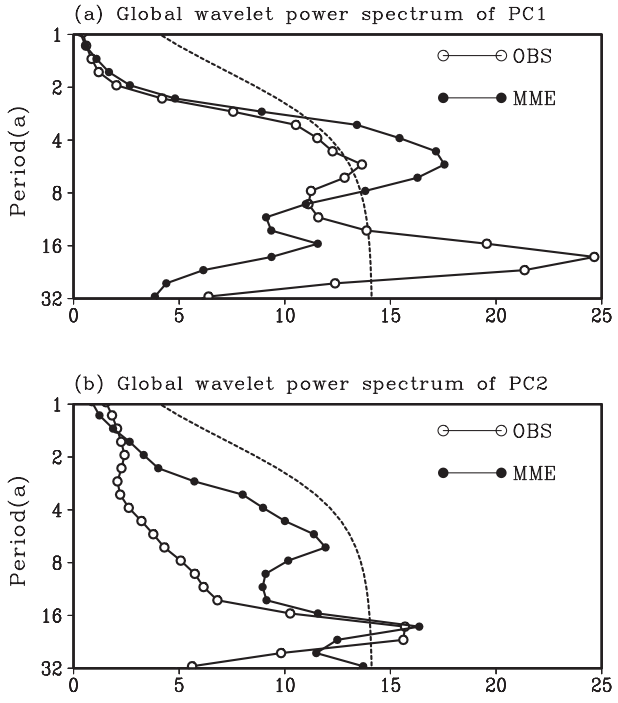

Fig. 9. The global power spectrum of the principal components (PCs) for (a) the first and (b) the second PC corresponding to the SVD modes in the SST anomalous filed. The observed (12-model ensemble) is indicated by the solid line with open circle (closed circle), and the black dashed line shows its significance at the 0.05 level.

Although our analyses potentially support the assumption that the frequent occurrence of CPEl Niño may result from natural climate variation, further investigations are still required concerning the detailed dynamics of CP-ENSO. Particularly, a focus is needed on explaining why CP-ENSO occurs more frequently in some decades but not in others under scenarios both with and without global warming. The answers to these questions will help us to understand the causes of the recent frequent occurrence of CP-ENSO events.

Acknowledgements. The authors acknowledge the anonymous reviewers for their helpful comments and suggestions. This study was jointly supported by the National Natural Science Foundation of China (Grant Nos. 41221064, 41376020, 41376025, and 90711003), the key program of 2012Z001 and 2013Z002 in the Chinese Academy of Meteorological Science, and the "Strategic Priority Research Program–Climate Change: Carbon Budget and Relevant Issues" of the Chinese Academy of Sciences (Grant No. XDA05090400). This study was also supported by the Jiangsu Collaborative Innovation Center for Climate Change.

REFERENCES

Allan, R., and T. Ansell, 2006: A new globally complete monthly historical gridded mean sea level pressure dataset (HadSLP2): 1850–2004. *J. Climate*, **19**, 5816–5842, doi: 10.1175/jcli3937.1.

Ashok, K., S. K. Behera, S. A. Rao, H. Y. Weng, and T. Yamagata, 2007: El Niño Modoki and its possible teleconnection. *J. Geophys. Res.*, **112**, C11007, doi: 10.1029/2006JC003798.

Ashok, K., C. Y. Tam, and W. J. Lee, 2009: ENSO Modoki impact on the Southern Hemisphere storm track activity during extended austral winter. *Geophys. Res. Lett.*, **36**, L12705, doi: 10.1029/2009GL038847.

Battisti, D. S., and A. C. Hirst, 1989: Interannual variability in a tropical atmosphereocean model: Influence of the basic

state, ocean geometry and nonlinearity. *J. Atmos. Sci.*, **46**(12), 1687–1712.

Bjerknes, J., 1969: Atmospheric teleconnections from the Equatorial Pacific. *Mon. Wea. Rev.*, **97**, 163–172, doi: 10.1175/1520-0493(1969)097<0163:atftep>2.3.co;2.

Choi, J., S.-I. An, and S.-W. Yeh, 2012: Decadal amplitude modulation of two types of ENSO and its relationship with the mean state. *Climate Dyn.*, **38**, 2631–2644, doi: 10.1007/s00382-011-1186-y.

Fu, C. B., H. F. Diaz, and J. O. Fletcher, 1986: Characteristics of the response of sea surface temperature in the central Pacific associated with warm episodes of the Southern Oscillation. *Mon. Wea. Rev.*, **114**(9), 1716–1739.

Giese, B. S., and S. Ray, 2011: El Niño variability in simple ocean data assimilation (SODA), 1871–2008. *J. Geophys. Res.*, **116**, C02024, doi: 10.1029/2010jc006695.

Ham, Y.-G., and J.-S. Kug, 2011: How well do current climate models simulate two types of El Niño? *Climate Dyn.*, **39**, 383–398, doi: 10.1007/s00382-011-1157-3.

Jin, F.-F., 1997a: An equatorial ocean recharge paradigm for ENSO. Part I: Conceptual model. *J. Atmos. Sci.*, **54**, 811–829.

Jin, F.-F., 1997b: An equatorial ocean recharge paradigm for ENSO. Part II: Astripped-down coupled model. *J. Atmos. Sci.*, **54**, 830–847.

Kao, H.-Y., and J.-Y. Yu, 2009: Contrasting eastern-Pacific and central-Pacific types of ENSO. *J. Climate*, **22**(3), 615–632, doi: 10.1175/2008jcli2309.1.

Kim, S. T., and J.-Y. Yu, 2012: The two types of ENSO in CMIP5 models. *Geophys. Res. Lett.*, **39**, L11704, doi: 10.1029/2012gl052006.

Kug, J.-S., F.-F. Jin, and S.-I. An, 2009: Two types of El Niño events: cold tongue El Niño and warm pool El Niño. *J. Climate*, **22**, 1499–1515.

Kug, J.-S., Y.-G. Ham, J.-Y. Lee, and F.-F. Jin, 2012: Corrigendum: Improved simulation of two types of El Niño in CMIP5 models. *Environ. Res. Lett.*, **7**, 039502, doi: 10.1088/1748-9326/7/3/039502.

Larkin, N. K., and D. E. Harrison, 2005: On the definition of El Niño and associated seasonal average U.S. weather anomalies. *Geophys. Res. Lett.*, **32**, L13705, doi: 10.1029/2005gl022738.

Lee, T., and M. J. McPhaden, 2010: Increasing intensity of El Niño in the central-equatorial Pacific. *Geophys. Res. Lett.*, **37**, L14603, doi: 10.1029/2010gl044007.

McPhaden, M. J., T. Lee, and D. McClurg, 2011: El Niño and its relationship to changing background conditions in the tropical Pacific Ocean. *Geophys. Res. Lett.*, **38**, L15709, doi: 10.1029/2011gl048275.

Philander, S. G. H., T. Yamagata, and R. C. Pacanowski, 1984: Unstable air-sea interactions in the Tropics. *J. Atmos. Sci.*, **41**, 604–613.

Rasmusson, E. M., and T. H. Carpenter, 1982: Variations in tropical sea surface temperature and surface wind fields associated with the Southern Oscillation/El Niño. *Mon. Wea. Rev.*, **110**, 354–384.

Rayner, N. A., and Coauthors, 2003: Global analyses of sea surface temperature, sea ice, and night marine air temperature since the late nineteenth century. *J. Geophys. Res.*, **108**(D14), 4407, doi: 10.1029/2002jd002670.

Ren, H.-L., and F.-F. Jin, 2011: Niño indices for two types of ENSO. *Geophys. Res. Lett.*, **38**, L04704, doi: 10.1029/2010gl046031.

Schopf, P. S., and M. J. Suarez, 1988: Vacillations in a coupled oceanatmosphere model. *J. Atmos. Sci.*, **45**(3), 549–566.

Taylor, K. E., R. J. Stouffer, and G. A. Meehl, 2012: An overview of CMIP5 and the experiment design. *Bull. Amer. Meteor. Soc.*, **93**, 485–498.

Trenberth, K. E., and D. P. Stepaniak, 2001: Indices of El Niño evolution. *J. Climate*, **14**, 1697–1701.

Wang, C. Z., and X. Wang, 2013a: Classifying El Niño Modoki I and II by different impacts on rainfall in Southern China and typhoon tracks. *J. Climate*, **26**, 1322–1338, doi: 10.1175/jcli-d-12-00107.1.

Wang, D. X., Y. H. Qin, X. J. Xiao, Z. Q. Zhang, and X. Y. Wu, 2012: El Niño and El Niño Modoki variability based on a new ocean reanalysis. *Ocean Dyn.*, **62**, 1311–1322.

Wang, X., and C. Z. Wang, 2013b: Different impacts of various El Niño events on the Indian Ocean Dipole *Climate Dyn.*, doi: 10.1007/s00382-013-1711-2.

Wang, X., D. X. Wang, and W. Zhou, 2009: Decadal variability of twentieth century El Niño and La Niña occurrence from observations and IPCC AR4 coupled models. *Geophys. Res. Lett.*, **36**, L11701, doi: 10.1029/2009GL037929.

Weng, H. Y., K. Ashok, S. K. Behera, S. A. Rao, and T. Yamagata, 2007: Impacts of recent El Niño Modoki on dry/wet conditions in the Pacific rim during boreal summer. *Climate Dyn.*, **29**, 113–129, doi: 10.1007/s00382-007-0234-0.

Wyrtki, K., 1975: El Niño—The dynamic response of the equatorial Pacific oceanto atmospheric forcing. *J. Phys. Oceanogr.*, **5**, 572–584.

Xiang, B. Q., B. Wang, and T. Li, 2013: A new paradigm for the predominance of standing central pacific warming after the late 1990s. *Climate Dyn.* **41**(2), 327–340, doi: 10.1007/s00382-012-1427-8.

Xu, K., C. W. Zhu, and J. H. He, 2012: Linkage between the dominant modes in Pacific subsurface ocean temperature and the two type ENSO events. *Chinese Science Bulletin*, **57**, 3491–3496, doi: 10.1007/s11434-012-5173-4.

Xu, K., C. W. Zhu, and J. H. He, 2013: Two types of El Niño-related Southern Oscillation and their different impacts on global land precipitation. *Adv. Atmos. Sci.*, **30**, 1743–1757, doi: 10.1007/s00376-013-2272-3.

Yeh, S.-W., J.-S. Kug, B. Dewitte, M.-H. Kwon, B. P. Kirtman, and F.-F. Jin, 2009: El Niño in a changing climate. *Nature*, **461**, 511-514, doi: 10.1038/nature08316.

Yu, J.-Y., and H.-Y. Kao, 2007: Decadal changes of ENSO persistence barrier in SST and ocean heat content indices: 1958–2001. *J. Geophys. Res.*, **112**, D13106, doi: 10.1029/2006jd007654.

Yu, J.-Y., and S. T. Kim, 2010: Identification of central-pacific and Eastern-Pacific types of ENSO in CMIP3 models. *Geophys. Res. Lett.*, **37**, doi: 10.1029/2010GL044082.

Yu, J.-Y., and S. T. Kim, 2013: Identifying the types of major El Niño events since 1870. *Int. J. Climatol.*, **33**, 2105–2112, doi: 10.1002/joc.3575.

Yu, J.-Y., H.-Y. Kao, and T. Lee, 2010: Subtropics-related interannual sea surface temperature variability in the Central Equatorial Pacific. *J. Climate*, **23**, 2869–2884, doi: 10.1175/2010jcli3171.1.